



**HAL**  
open science

## Probing Colossal Carbon Rings

Samuel J.P. Marlton, Jack Buntine, Patrick Watkins, Chang Liu, Ugo Jacovella, Eduardo Carrascosa, James Bull, Evan Bieske

► **To cite this version:**

Samuel J.P. Marlton, Jack Buntine, Patrick Watkins, Chang Liu, Ugo Jacovella, et al.. Probing Colossal Carbon Rings. *Journal of Physical Chemistry A*, 2023, 127 (5), pp.1168-1178. 10.1021/acs.jpca.2c07068 . hal-04505592

**HAL Id: hal-04505592**

**<https://hal.science/hal-04505592v1>**

Submitted on 15 Mar 2024

**HAL** is a multi-disciplinary open access archive for the deposit and dissemination of scientific research documents, whether they are published or not. The documents may come from teaching and research institutions in France or abroad, or from public or private research centers.

L'archive ouverte pluridisciplinaire **HAL**, est destinée au dépôt et à la diffusion de documents scientifiques de niveau recherche, publiés ou non, émanant des établissements d'enseignement et de recherche français ou étrangers, des laboratoires publics ou privés.

# Probing Colossal Carbon Rings

Samuel J.P. Marlton,<sup>†</sup> Jack T. Buntine,<sup>†</sup> Patrick Watkins,<sup>†</sup> Chang Liu,<sup>†</sup> Ugo

Jacovella,<sup>‡</sup> Eduardo Carrascosa,<sup>¶</sup> James N. Bull,<sup>§</sup> and Evan J. Bieske<sup>\*,†</sup>

<sup>†</sup>*School of Chemistry, The University of Melbourne, Victoria, Australia 3010*

<sup>‡</sup>*Université Paris-Saclay, CNRS, Institut des Sciences Moléculaires d'Orsay, 91405 Orsay,*

*France*

<sup>¶</sup>*Bruker Daltonics GmbH & Co. KG, Fahrenheitstrasse 4, 28359 Bremen, Germany*

<sup>§</sup>*School of Chemistry, Norwich Research Park, University of East Anglia, Norwich NR4*

*7TJ, United Kingdom*

E-mail: [evanjb@unimelb.edu.au](mailto:evanjb@unimelb.edu.au)

## Abstract

Carbon aggregates containing between 10 and 30 atoms preferentially arrange themselves as planar rings. To learn more about this exotic allotrope of carbon, electronic spectra are measured for even cyclo[*n*]carbon radical cations ( $C_{14}^+ - C_{36}^+$ ) using two-color photodissociation action spectroscopy. To eliminate spectral contributions from other isomers, the target cyclo[*n*]carbon radical cations are isomer-selected using a drift tube ion mobility spectrometer prior to spectroscopic interrogation. The electronic spectra exhibit sharp transitions spanning the visible and near infrared spectral regions with the main absorption band shifting progressively to longer wavelength by  $\approx 100$  nm for every additional two carbon atoms. This behaviour is rationalised with a Hückel theory model describing the energies of the in-plane and out-of-plane  $\pi$  orbitals. Photoexcitation of smaller carbon rings leads preferentially to neutral  $C_3$  and  $C_5$  loss, whereas rings larger than  $C_{24}^+$  tend to also decompose into two smaller rings, which,

1  
2  
3 when possible, have aromatic stability. Generally, the observed charged photofrag-  
4  
5 ments correspond to low energy fragment pairs, as predicted by density functional  
6  
7 theory calculations (CAM-B3LYP-D3(BJ)/cc-pVDZ). Using action spectroscopy it is  
8  
9 confirmed that  $C_{14}^+$  and  $C_{18}^+$  photofragments from  $C_{28}^+$  rings have cyclic structures.

## 13 Introduction

16 Widespread acceptance that assemblies of carbon atoms adopt structures besides the famil-  
17  
18 iar graphite and diamond allotropes followed the discovery of the  $C_{60}$  fullerene cluster and  
19  
20 progressed with the synthesis of other fullerenes, carbon nanotubes and graphene.<sup>1-3</sup> Even  
21  
22 before the discovery of fullerenes, it was proposed that the smaller carbon clusters exist  
23  
24 predominately as linear chains, with rings (also known as cyclo[ $n$ ]carbons) becoming the  
25  
26 dominant isomer at  $n \approx 10$  when the stabilization accompanying formation of an additional  
27  
28 C-C bond outweighs the energetic penalty associated with bending the chain.<sup>4,5</sup> Charged  
29  
30 carbon rings were probably first observed, without being recognised as such, by Hahn and  
31  
32 coworkers in 1942 in mass spectra of ions produced in discharges between carbon electrodes,<sup>6</sup>  
33  
34 and were later deduced to exist through gas-phase reactivity studies.<sup>7,8</sup> Subsequent ion mobil-  
35  
36 ity studies of  $C_n^+$  and  $C_n^-$  clusters formed by laser ablation of graphite provided compelling  
37  
38 evidence for the existence of rings over the  $n=10-80$  range, with rings being progressively  
39  
40 supplanted as the dominant isomer by bi-rings (from  $C_{22}^+$ ) and fullerenes (from  $C_{32}^+$ ).<sup>9-13</sup>  
41  
42 Examples of the co-existing ring, bi-ring and fullerene isomers are shown in Figure 1(a).  
43  
44 The general chemical significance of cyclo[ $n$ ]carbons is emphasized by the fact that they are  
45  
46 formed through diverse routes, including by laser ablation of graphite, the decomposition  
47  
48 of chlorinated polycyclic aromatic hydrocarbons (PAHs),<sup>14</sup> and the photoinduced dehydro-  
49  
50 genation of PAHs.<sup>15-17</sup> Recently, in the culmination of longstanding efforts,<sup>18,19</sup> neutral  $C_{18}$   
51  
52 cyclo[ $n$ ]carbons were synthesized on a surface and imaged individually using STM/AFM,  
53  
54 demonstrating that the ring has polyynic rather than cumulenic bonding.<sup>19</sup>

56 Although there have been many theoretical investigations of cyclo[ $n$ ]carbons,<sup>2-5,20-23</sup> fo-

1  
2  
3  
4 cusing mainly on their structures and stabilities, experimental data against which the calcu-  
5 lations can be compared and calibrated are rare. In this study we explore the photophysical  
6 and photochemical properties of charged, even cyclo[ $n$ ]carbon cations up to  $C_{36}^+$  in the  
7 gas phase, measuring electronic spectra, and investigating their decomposition following ab-  
8 sorption of ultraviolet light. Earlier studies in which electronic spectra were measured for  
9 mass-selected rings up to  $C_{28}^+$  tagged with  $N_2$  molecules,<sup>24</sup> and with He atoms,<sup>25</sup> showed  
10 that even cyclo[ $n$ ]carbon cations possess relatively sharp absorption bands over the visi-  
11 ble (Vis) and near infrared (NIR) ranges, with a progressive linear shift of the strongest  
12 absorptions to longer wavelength by  $\approx 100$  nm for each additional two C atoms. Our prelim-  
13 inary investigations of the odd  $C_{2n+1}^+$  rings indicate that the wavelengths of their electronic  
14 absorption bands do not fit with the trends established for the even  $C_{2n}^+$  rings.

15  
16 Here, we extend the earlier spectroscopic studies in several ways. First, we obtain elec-  
17 tronic spectra of bare  $C_{2n}^+$  carbon rings ( $C_{14}^+ - C_{36}^+$ ) without attached tag atoms or  
18 molecules. Electronic spectra of the bare carbon rings along with previously reported  $C_{2n}^+$ -  
19  $He_m$  and  $C_{2n}^+-(N_2)_m$  spectra allow us to assess the shifts caused by attached He atoms and  
20  $N_2$  molecules, which are not known *a priori*. Wavelengths for the absorption peaks of the  
21 bare carbon clusters can be compared directly with astronomical data to decide whether  
22 cyclo[ $n$ ]carbon cations exist in circumstellar and interstellar regions and whether their ab-  
23 sorptions correspond to any diffuse interstellar bands (DIBs). Furthermore, spectra for larger  
24 carbon ring cations,  $C_{30}^+$ ,  $C_{32}^+$ ,  $C_{34}^+$  and  $C_{36}^+$ , which have not been reported previously,  
25 allow us to investigate whether spectral patterns apparent for the smaller rings (up to  $C_{28}^+$ )  
26 persist for larger clusters. Probing the larger clusters ( $C_{28}^+$  and above) presents challenges  
27 due to the coexistence of ring, bi-ring and fullerene isomers.<sup>9-12,24</sup> To address this issue,  
28 the carbon clusters are selected according to both their mass and their isomeric structure  
29 (using ion mobility) *prior* to spectroscopic interrogation, eliminating ambiguity in the size  
30 and structure of the species being probed.

31  
32  
33  
34  
35  
36  
37  
38  
39  
40  
41  
42  
43  
44  
45  
46  
47  
48  
49  
50  
51  
52  
53  
54  
55  
56  
57  
58  
59  
60  
Ideally, electronic spectra of the carbon ring cations would be understood with the aid

of electronic structure calculations. However, there is considerable debate over appropriate methods for describing even the ground electronic state properties of carbon rings,<sup>5,20–23</sup> so that reliably predicting wavelengths and intensities for electronic transitions of even smaller rings will be challenging, while reliable predictions for the larger rings are certainly currently not feasible. As a first step to understanding the electronic absorptions of carbon rings, we develop a simple model based on Hückel theory, describing the valence electrons occupying in-plane and out-of-plane  $\pi$  orbitals (Figure 1(b)). The model is consistent with the linear relationship between absorption wavelength and cluster size that was found to apply for even cyclo[ $n$ ]carbon cations up to  $C_{28}^+$ .<sup>24,25</sup>

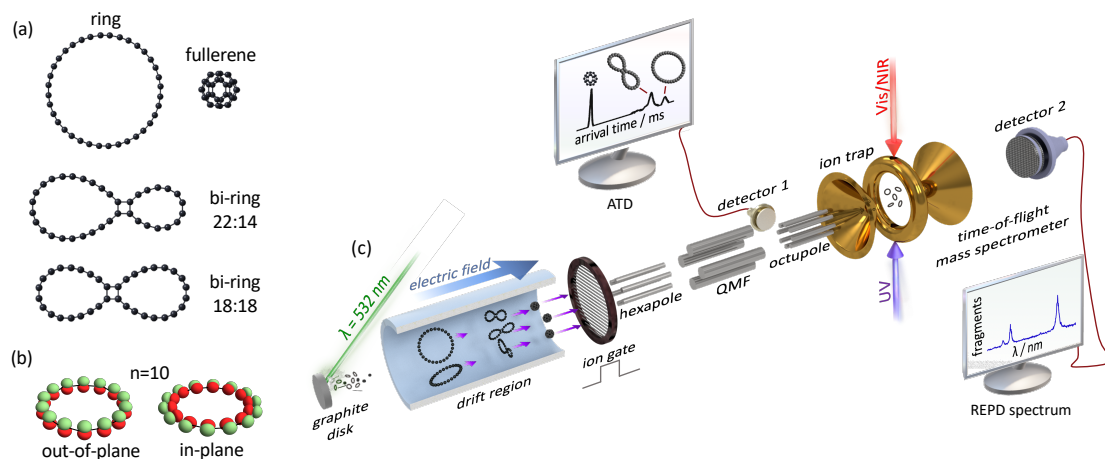


Figure 1: (a) Structures of  $C_{36}^+$  isomers – ring, 18:18 and 22:14 bi-rings, and fullerene. (b) Lowest energy out-of-plane and in-plane  $\pi$  molecular orbitals for  $C_{10}$ . (c) Experimental strategy for spectroscopically probing mobility-selected carbon rings. Charged carbon clusters generated by pulsed laser ablation of a graphite disk are separated according to their collision cross sections with He buffer gas before passing through a quadrupole mass filter (QMF). An arrival time distribution (ATD), which shows peaks due to different isomers, can be measured by monitoring the ion signal at detector 1. For spectroscopy experiments, the target cyclo[ $n$ ]carbon isomer population is selected by an electrostatic gate at the end of the drift tube, opened at an appropriate delay with respect to the ablation laser pulse, followed by mass selection with a quadrupole mass filter (QMF). The cyclo[ $n$ ]carbon cations are introduced into a cryogenically cooled ion trap where they are spectroscopically probed using 2-colour resonance enhanced photodissociation (see Figure 2). An electronic spectrum is recorded by monitoring the photofragment intensity at detector 2 as a function of the wavelength of the Vis/NIR beam. A comprehensive description of the apparatus is given in refs. 24 and 26.

1  
2  
3  
4 To learn more about the  $C_{14}^+ - C_{36}^+$  rings and to complement the spectroscopic studies,  
5 we have also investigated their photofragmentation behaviour. There have been several pre-  
6 vious photodissociation studies of carbon clusters cations in the  $n=14-20$  range (presumably  
7 rings), demonstrating that they mainly lose neutral  $C_3$  or  $C_5$  photofragments.<sup>27-31</sup> Photodis-  
8 sociation studies for larger rings in the  $C_{22}^+ - C_{36}^+$  range are potentially complicated by the  
9 presence of coexisting isomers – rings and bi-rings for  $C_{22}^+ - C_{30}^+$ , and rings, bi-rings and  
10 fullerenes for  $C_{32}^+ - C_{36}^+$ . For example, Smalley and co-workers found that the photofrag-  
11 ment distribution for  $C_{36}^+$  depended on light intensity and on ion source conditions, which  
12 was taken as evidence for coexisting fullerene isomers (losing  $C_2$  units) and non-fullerene  
13 isomers (giving  $C_n^+$  photofragments in the  $n=14-22$  range).<sup>29</sup> Later, Misaizu and coworkers  
14 addressed the isomeric ambiguity in photodissociation studies of  $C_{32}^+$ ,  $C_{34}^+$  and  $C_{36}^+$ , sepa-  
15 rating fullerene and non-fullerene isomers in an ion mobility drift cell before irradiating them  
16 with 266 nm light.<sup>32</sup> For each cluster size, the two isomer families produced distinct photo-  
17 product ion distributions. However, in the ref. 29 and ref. 32 experiments, the non-fullerene  
18 population potentially contained ring and bi-ring isomers. To eliminate this ambiguity, we  
19 have adopted an isomer selective approach to probe  $C_{14}^+ - C_{36}^+$  rings. The resolution of our  
20 ion mobility stage is sufficient to cleanly separate the target rings from bi-rings and from  
21 fullerenes prior to photodissociation. To help interpret the observed photofragment distri-  
22 butions, relative energies of fragment pairs are calculated using density functional theory  
23 (DFT), allowing us to explore whether the preferred charged photofragments correspond to  
24 the lower energy fragment channels.

25  
26  
27  
28  
29  
30  
31  
32  
33  
34  
35  
36  
37  
38  
39  
40  
41  
42  
43  
44  
45  
46  
47  
48  
49  
50  
51  
52  
53  
54  
55  
56  
57  
58  
59  
60  
Despite the many measurements for photofragment distributions from charged carbon  
clusters, there have been no direct determinations of the fragments' structures (linear, ring,  
bi-ring or fullerene). In principle, the photofragment structures could be probed using a  
tandem ion mobility arrangement, with photoexcitation of the  $C_n^+$  clusters after the first ion  
mobility stage, and separation of photofragment isomers in the second ion mobility stage.<sup>33</sup>  
Here we use an alternative spectroscopically-based strategy to investigate the structures of

1  
2  
3 the main  $C_{14}^+$  and  $C_{18}^+$  photofragments generated from  $C_{28}^+$ . The nascent photofragments  
4 are trapped, tagged with  $N_2$  molecules, and irradiated with tunable radiation to record their  
5 characteristic electronic spectra.  
6  
7  
8  
9

## 10 11 12 Methods

13  
14  
15 Obtaining electronic or infrared spectra of larger cyclo[ $n$ ]carbon cations entails dealing with  
16 complications associated with the presence of different isomers (rings, bi-rings and fullerenes),  
17 whose spectra may be entangled. To address this issue, we have developed an isomer-selective  
18 approach for measuring electronic spectra.<sup>24,26,34</sup> The experimental arrangement is shown  
19 schematically in Figure 1(c) and is described in more detail in refs. 24 and 26.  
20  
21  
22  
23

24  
25 Carbon cluster cations were generated by laser ablation of a rotating graphite disk using  
26 the focused, frequency-doubled output of a pulsed Nd:YAG laser ( $\lambda=532$  nm, 12 mJ/pulse,  
27 100 Hz repetition rate). The ablation source is situated at the beginning of a drift tube  
28 ion mobility spectrometer which was used to separate the charged carbon clusters according  
29 to their drift time through He buffer gas ( $P\approx 3$  Torr). The target cyclo[ $n$ ]carbon cations  
30 could be selected at the end of the drift tube using a pulsed electrostatic ion gate opened  
31 at an appropriately timed delay and duration. Following the ion gate, the charged clusters  
32 were collected by an RF ion funnel and passed through a 1 mm orifice into an RF hexapole  
33 ion guide (pressure typically  $5\times 10^{-5}$  Torr), which was used to accumulate ions from 50  
34 ablation laser pulses over 0.5 s. After emerging from the hexapole, the ions travelled through  
35 a quadrupole mass filter where they were mass selected and then passed through an octupole  
36 ion guide and into a cryogenically cooled quadrupole ion trap (QIT). Pulses of either He gas  
37 or He/ $N_2$  100:1 gas mixture were injected at 2 Hz, with the gas pulse initiated 10–20 ms  
38 before arrival of the ion packet. The temperature of the trap ( $T\approx 10$  K) was measured using  
39 a Lakeshore DT-670 silicon diode. The actual temperature of the ions in the QIT is likely  
40 to be slightly higher than the trap temperature due to RF heating.  
41  
42  
43  
44  
45  
46  
47  
48  
49  
50  
51  
52  
53  
54  
55  
56  
57  
58  
59  
60

1  
2  
3  
4  
5  
6  
7  
8  
9  
10  
11  
12  
13  
14  
15  
16  
17  
18  
19  
20  
21  
22  
23  
24  
25  
26  
27  
28  
29  
30  
31  
32  
33  
34  
35  
36  
Electronic spectra of the  $C_{2n}^+$  ( $n=7-18$ ) clusters were obtained by 2-colour resonance enhanced photodissociation or through 1-colour resonance enhanced photodissociation of  $C_{2n}^+$ - $(N_2)_m$  complexes. Alternate packets of ions in the QIT were exposed to pulses of unfocused, wavelength-tunable light from an optical parametric oscillator (OPO, EKSPLA NT342B,  $\leq 1 \text{ mJ/cm}^2/\text{pulse}$ , 6 ns pulse width, bandwidth  $\approx 4 \text{ cm}^{-1}$ ). Each tunable wavelength pulse was followed 10 ns later by a pulse of fixed wavelength UV light (OPO, EKSPLA NT342B,  $\leq 1 \text{ mJ/cm}^2/\text{pulse}$ , 6 ns pulse width, bandwidth  $\approx 8 \text{ cm}^{-1}$ ), which served to dissociate the excited clusters. For clusters up to  $C_{26}^+$ , charged fragments corresponding to  $C_3$  or  $C_5$  loss were monitored, whereas for  $C_{28}^+$  and larger clusters,  $C_{14}^+$  or  $C_{18}^+$  photofragments were monitored. The wavelength and power of the UV beam were adjusted to maximize the resonance enhanced photodissociation signal from the first tunable light pulse while minimizing background photofragmentation. We attempted to avoid saturating the transitions by adjusting the intensity of the first laser pulse so that  $\leq 5\%$  of the ions were dissociated. After 480 ms the ions were ejected from the QIT into a linear time-of-flight (ToF) mass spectrometer (length 0.9 m). Electronic spectra were obtained by plotting the charged photofragment signal as a function of wavelength with intensities normalised by OPO power. Wavelength calibration was accomplished with a wavemeter (High Finesse, LSA).

37  
38  
39  
40  
41  
42  
43  
44  
45  
46  
47  
48  
49  
50  
51  
52  
53  
54  
55  
56  
57  
58  
59  
60  
Geometries of  $C_{2n}^+$  clusters were optimised using density functional theory, employing the range separated CAM-B3LYP functional<sup>35</sup> with the cc-pVDZ basis set<sup>36</sup> and empirical dispersion (D3BJ)<sup>37</sup> using Gaussian16.<sup>38</sup> As shown in Section S1 of the SI, the dissociation energies and ionization energies of the carbon clusters calculated using the CAM-B3LYP-D3(BJ)/cc-pVDZ approach compare reasonably well with available experimental data.<sup>39-41</sup> For the  $C_{11}^+$ - $C_{18}^+$  clusters our calculations reproduce the observed variation of dissociation energies with cluster size reported in ref. 39, although the calculated dissociation energies are larger than the experimental dissociation energies by between 5% and 23%. For  $C_{11}^+$ - $C_{15}^+$  clusters our calculations underestimate the experimental ionization energies reported in ref. 40 by between 4% and 17%. The CAM-B3LYP-D3(BJ)/cc-pVDZ method yields



1  
2  
3 similar dissociation and ionization energies to previous calculations, which employed the  
4 B3LYP/def2-TZVPP method,<sup>31</sup> and the high level CCSD(T)/cc-pVQZ method.<sup>40</sup> High level  
5 methods such as CCSD(T) are too expensive for the larger carbon clusters targeted in this  
6 study. The CAM-B3LYP-D3(BJ)/cc-pVDZ method provides a good compromise between  
7 cost and accuracy, and is employed for all investigated carbon species (from C to C<sub>36</sub>).  
8  
9  
10  
11  
12  
13  
14

## 15 Results and Discussion

### 19 Electronic spectra of even cyclo[*n*]carbon cations

20  
21 The rich and potentially confusing mixture of carbon cluster isomers generated by laser ab-  
22 lation of graphite is illustrated in Figure 2(a), which shows arrival time distributions (ATDs)  
23 for even C<sub>14</sub><sup>+</sup>–C<sub>36</sub><sup>+</sup> clusters driven by an electric field through a drift region containing he-  
24 lium buffer gas (signal recorded at detector 1 in Figure 1(c)). The more prominent peaks in  
25 the ATDs are due to rings, bi-rings, and fullerenes (single and multiply charged), as observed  
26 in previously reported ATDs of carbon cluster cations.<sup>9,11,12</sup> We find that clusters between  
27 C<sub>10</sub><sup>+</sup> and C<sub>28</sub><sup>+</sup> are predominately monocyclic rings and that monocyclic rings persist at least  
28 up to C<sub>40</sub><sup>+</sup> (see Figure 2(a)). Bi-ring clusters become increasingly apparent from their onset  
29 at C<sub>22</sub><sup>+</sup> and are more abundant than rings above C<sub>30</sub><sup>+</sup> (depending on ion source conditions).  
30 Bi-rings are predicted to consist of two rings linked by a four-membered ring, as shown  
31 in Figure 1(a).<sup>42</sup> The ATD peaks for bi-rings are broader and more asymmetric than the  
32 ring peaks, presumably because carbon atoms can be distributed in different ways between  
33 the two rings, giving several bi-ring isomers with different collision cross sections (see Fig-  
34 ure 1(a)).<sup>42</sup> Fullerenes first become apparent for C<sub>28</sub><sup>+</sup> (very low abundance) and constitute  
35 the main isomer for C<sub>36</sub><sup>+</sup> and larger clusters.  
36  
37  
38  
39  
40  
41  
42  
43  
44  
45  
46  
47  
48  
49  
50

51 It is evident from Figure 2(a) that for carbon cluster cations larger than C<sub>26</sub><sup>+</sup>, there  
52 are two or more isomers with comparable abundances (ring, bi-ring, and single and mul-  
53 tiply charged fullerenes), and that to avoid isomeric ambiguity it is essential to select the  
54  
55  
56  
57  
58  
59  
60

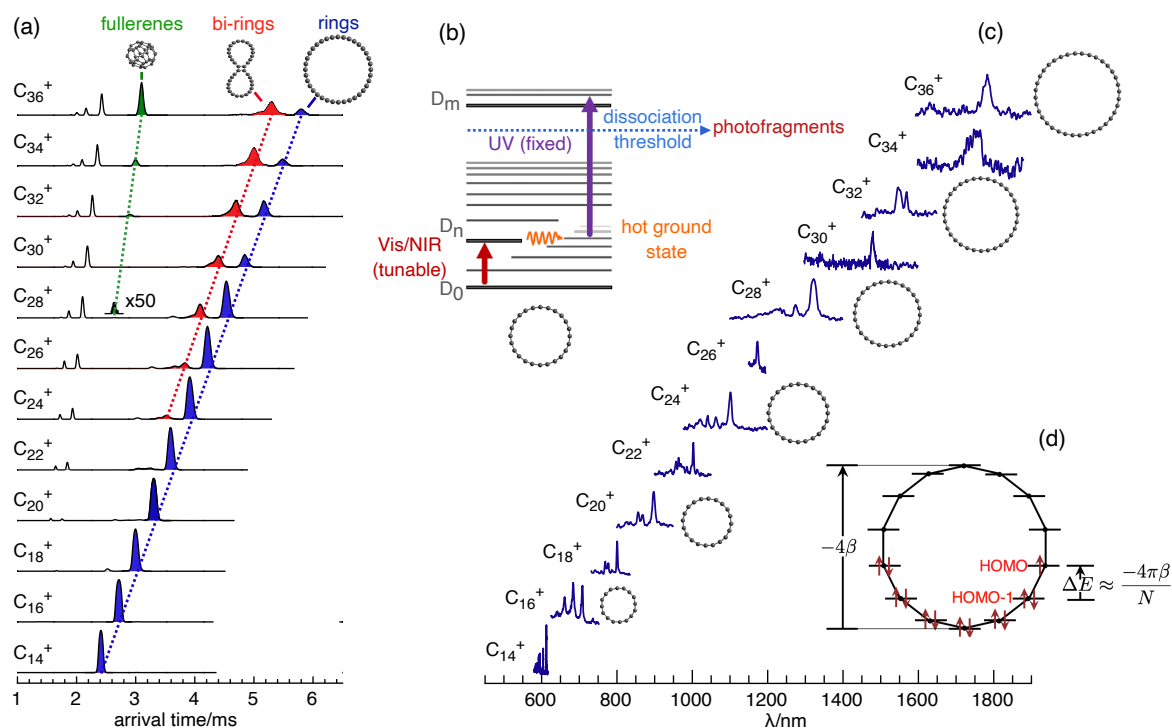


Figure 2: (a) ATDs for carbon cluster cations generated by 532 nm laser ablation of a graphite disk monitoring the ion signal at detector 1 (see Figure 1(c)). Peaks due to rings, bi-rings and fullerenes are highlighted in blue, red and green, respectively. Unlabelled peaks at shorter arrival time are due to larger fullerenes bearing multiple charges. (b) 2-colour resonance enhanced photodissociation scheme for obtaining electronic spectra. (c) Electronic spectra of  $C_{14}^+$ – $C_{36}^+$  rings. The target cyclo[ $n$ ]carbon clusters (blue peaks in (a)) were mobility-selected following the drift region of the apparatus using the pulsed electrostatic ion gate (see Figure 1(c)) before being probed using the scheme shown in (b). (d) Frost-Musulin diagram showing Hückel energies for in-plane  $\pi$  orbitals of  $C_{14}^+$ .

target isomer population *prior* to spectroscopic interrogation. This is accomplished using an electrostatic ion gate at the end of the drift region that is opened at appropriate delay and duration to pass ions with a narrow range of collision cross sections (see Figure 1(c)). These ions subsequently pass through a quadrupole mass filter tuned to the mass of the desired target ion and then into a cryogenically cooled quadrupole ion trap where they are spectroscopically probed using the 2-color resonance enhanced photodissociation (REPD) scheme shown in Figure 2(b). For more details see ref. 26, which describes separation and spectroscopic interrogation of ring and bi-ring isomers of  $C_{28}^+$ .

1  
2  
3  
4 Electronic spectra of isomer-selected even  $C_{14}^+ - C_{36}^+$  radical cation rings (blue peaks in  
5 Figure 2(a)) are shown in Figure 2(c). Each spectrum shown in Figure 2(c) is the average of  
6 4 or more individual scans. In each case the observed band presumably corresponds to the  
7 lowest energy transition with appreciable intensity that proceeds from the doublet ground  
8 state to a doublet excited state. As explained below, in a Hückel picture the transition  
9 would correspond to promotion of an electron from the HOMO-1 to the HOMO for the  
10 in-plane  $\pi$  system (Figure 2(d)). Wavelengths for the main transitions for the  $C_{2n}^+$  clusters  
11 are listed in Table 1. The  $C_{14}^+ - C_{28}^+$  spectra exhibit similar vibronic structure to the  
12 structure observed in previously reported spectra for  $C_{2n}^+-(N_2)_m$  and  $C_{2n}^+-He_m$  clusters.<sup>24,25</sup>  
13 Electronic spectra of  $C_{30}^+$ ,  $C_{32}^+$ ,  $C_{34}^+$  and  $C_{36}^+$  clusters (tagged or untagged) have not been  
14 reported previously. Comparison of the absorption wavelengths for the  $C_{2n}^+$ ,  $C_{2n}^+-(N_2)_m$   
15 and  $C_{2n}^+-He_m$  clusters, show that the spectral shifts caused by He and  $N_2$  tags are relatively  
16 small and for the larger clusters (above  $C_{20}^+$ ) are less than the band widths. Shifts in the  
17 transitions of  $C_{14}^+$ , the cluster with the sharpest bands, are discussed in more detail below.  
18  
19  
20  
21  
22  
23  
24  
25  
26  
27  
28  
29  
30  
31  
32

33 A characteristic feature of the cation carbon rings is the regular wavelength shift of  
34 the main electronic transition by around 100 nm for each additional two carbon atoms.<sup>24</sup>  
35 This trend is illustrated in Figure 3(a), where wavelengths of the transitions are plotted as  
36 a function of cluster size. Another obvious aspect of the spectra shown in Figure 2(b) is  
37 the alternation of band widths with size – the aromatic  $C_{4k+2}^+$  clusters ( $C_{14}^+$ ,  $C_{18}^+$  etc.)  
38 have narrow bands, whereas bands of the anti-aromatic  $C_{4k}^+$  clusters ( $C_{16}^+$ ,  $C_{20}^+$  etc.) are  
39 broader. This alternation is apparent in Figure 3(b) where the widths of the origin transitions  
40 are plotted as a function of cluster size. Although the bandwidth alternation is quite evident  
41 for  $C_{14}^+$  to  $C_{30}^+$ , the situation is not so clear for  $C_{32}^+$ ,  $C_{34}^+$  and  $C_{36}^+$ . In particular,  
42 the  $C_{34}^+$  peak should be narrow based on the trend for the smaller clusters, but is instead  
43 very broad. However, it is worth noting that the  $C_{34}^+$  transition was difficult to obtain,  
44 and the transition may be somewhat saturated. The band-width alternation, which is also  
45  
46  
47  
48  
49  
50  
51  
52  
53  
54  
55  
56  
57  
58  
59  
60

Table 1: Measured origin transition wavelengths (nm in air) for bare  $C_n^+$  rings, for previously measured  $C_n^+-N_2$  clusters from ref. 24, for  $C_n^+-He$  clusters from ref. 25, and estimated for bare  $C_n^+$  clusters from ref. 25.

cluster	$C_n^{+a}$	$C_n^+-N_2^b$	$C_n^+-He^c$	$C_n^{+c}$ extrapolated
$C_{36}^+$	$1783 \pm 10$			
$C_{34}^+$	$1747 \pm 10$			
$C_{32}^+$	$1568.6 \pm 3.0$			
	$1545.6 \pm 3.0$			
$C_{30}^+$	$1477.6 \pm 3.0$			
$C_{28}^+$	$1321.6 \pm 3.0$	$1320.6 \pm 3.5$	$1323.4 \pm 0.7$	$1324.3 \pm 1$
$C_{26}^+$	$1171.8 \pm 3.0$	$1173.1 \pm 0.7$		
$C_{24}^+$	$1100.1 \pm 2.0$	$1099.3 \pm 2.4$	$1100.5 \pm 0.5$	$1101.2 \pm 0.9$
$C_{22}^+$	$1002.5 \pm 1.0$	$1001.6 \pm 0.5$	$1002.0 \pm 0.5$	$1002.5 \pm 0.6$
$C_{20}^+$	$897.5 \pm 1.0$	$898.6 \pm 1.6$	$896.8 \pm 0.5$	$897.2 \pm 0.6$
$C_{18}^+$	$799.0 \pm 1.0$	$797.5 \pm 0.3^d$	$799.1 \pm 0.5$	$799.5 \pm 0.6$
$C_{16}^+$	$709.2 \pm 1.0$	$709.5 \pm 1.0$	$708.6 \pm 0.5$	$708.8 \pm 0.5$
$C_{14}^+$	$612.7 \pm 0.1$	$611.9 \pm 0.2$	$612.4 \pm 0.1$	$612.6 \pm 0.2$

<sup>a</sup> this work. <sup>b</sup> ref. 24 <sup>c</sup> ref. 25. <sup>d</sup> wavelength for  $C_{28}^+-(N_2)_2$  transition

apparent in spectra of  $C_{2n}^+-(N_2)_m$  and  $C_{2n}^+-He_m$  clusters,<sup>24,25</sup> has been hypothesized as due to variations in the rate of non-radiative decay for the clusters<sup>24</sup> – the lowest quartet state, which may be involved in non-radiative deactivation, lies just above the doublet ground state for the anti-aromatic clusters, and somewhat higher in energy for the aromatic clusters.<sup>43</sup> With increasing cluster size, the excited doublet state drops in energy, necessarily reducing the gap with the lower lying quartet state. This may affect the coupling between excited doublet state and the quartet vibronic states for the larger clusters and may mean that isolated resonances play a greater role. For  $C_{32}^+$  there are actually two bands in the origin region spaced by  $95\text{ cm}^{-1}$ , with the higher energy band being  $\approx 3$  times stronger than the lower energy band. The cause of the band doubling is uncertain but may be associated with an interaction between the excited doublet state and another vibronic state (possibly a quartet state). It is also worth pointing out that the transition energies of  $C_{32}^+$ ,  $C_{34}^+$  and  $C_{36}^+$  are only 0.80, 0.71 and 0.70 eV, respectively, and lie in the energetic vicinity of vibrational

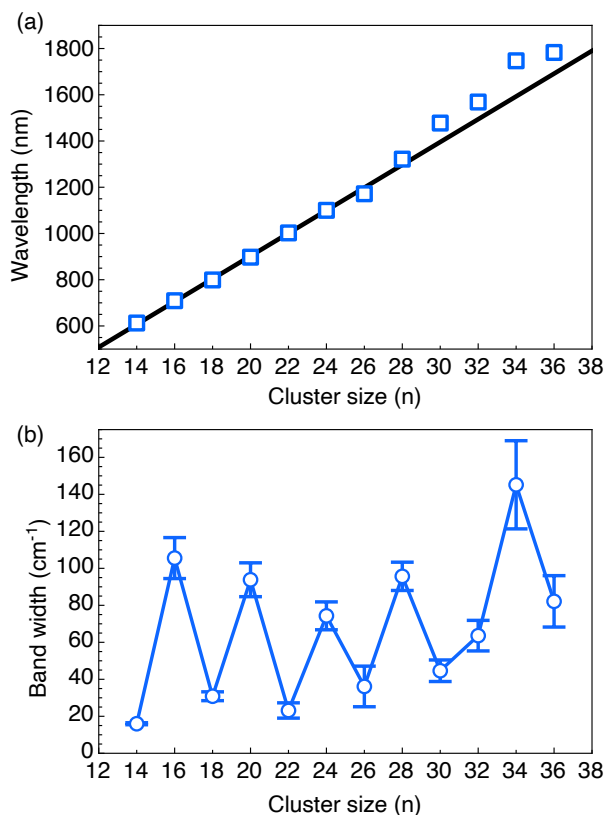


Figure 3: (a) Wavelengths for origin transitions of even cyclo[ $n$ ]carbon radical cations as a function of  $n$ . The linear fit is for  $C_{14}^+$  to  $C_{28}^+$  data. Absorptions of the larger clusters,  $C_{30}^+$  to  $C_{36}^+$ , occur to longer wavelength than expected from the linear trend established for the smaller clusters. (b) Widths of origin transitions as a function of cluster size. The plotted widths are based on Gaussian fits to the origin bands with error bars corresponding to twice the standard deviation of fit. There are two peaks in the origin transition region for  $C_{32}^+$  (see Table 1). The width of the broader peak ( $64 \pm 8 \text{ cm}^{-1}$ ) is reported in (b) while the narrower band has a width of  $26 \pm 6 \text{ cm}^{-1}$ .

levels involving 3 or 4 quanta of highest frequency C-C stretch modes, so resonances with vibrational levels associated with the ground electronic state may also be important.

## Hückel model for transition wavelengths of $C_{2n}^+$ rings

The linear shift of the transitions of the  $C_{2n}^+$  rings with cluster size can be rationalised using a simple Hückel theory model. The cyclo[ $n$ ]carbons possess an out-of-plane  $\pi$  orbital

1  
2  
3 system that is antisymmetric with respect to reflection in the molecular plane, and an orthog-  
4 onal in-plane  $\pi$  orbital system that is symmetric with respect to reflection in the molecular  
5 plane (see Figure 1(b)). These two  $\pi$  systems are identical in the limit of an infinitely large  
6 ring. However, for finite rings the overlap of the contributing in-plane atomic p orbitals is  
7 reduced due to ring curvature, so that each in-plane orbital lies slightly higher in energy  
8 than its counterpart out-of-plane orbital.<sup>44</sup> Therefore, in a Hückel framework, the HOMO  
9 for the cyclo[ $n$ ]carbons will be a singly occupied in-plane  $\pi$  orbital (see Figure 2(d)).<sup>45,46</sup> The  
10 lowest energy transition not involving promotion from an in-plane to an out-of-plane orbital  
11 (or *vice versa*) should correspond to promotion of an electron from the in-plane HOMO-1  
12 orbital to the in-plane HOMO orbital.

13  
14  
15 Energies,  $e_j$ , for the Hückel MOs for a ring of  $N$  carbon atoms are given by:<sup>45,46</sup>

$$e_j = \alpha + 2\beta \cos(2j\pi/N) \quad (1)$$

16  
17  
18 with  $j=0, \pm 1, \pm 2, \dots, \pm(\frac{N}{2} - 1), \frac{N}{2}$  for  $N$  even, and  $j=0, \pm 1, \pm 2, \dots, \pm\frac{N-1}{2}$  for  $N$  odd.  
19 Here,  $\alpha$  is the Coulomb integral and  $\beta$  is the resonance integral. Orbital energies for the  
20 cyclo[ $n$ ]carbons can be represented by Frost-Musulin diagrams as shown in Figure 2(d) for  
21  $C_{14}^+$ .<sup>46</sup> The circumscribing circle has a diameter of  $-4\beta$  and the length of the arc between  
22 adjacent points is  $-4\pi\beta/N$ .<sup>46</sup> It can be seen geometrically from Figure 2(d) that, as  $N$   
23 increases, the energy difference ( $\Delta E$ ) between the fully occupied HOMO-1 ( $e_{(N-2)/4}$ ) and  
24 partially occupied HOMO orbital ( $e_{(N-2)/4-1}$ ) is given approximately by:

$$\Delta E = e_{(N-2)/4} - e_{(N-2)/4-1} \approx -4\pi\beta/N \quad (2)$$

25  
26  
27 Equation 2 is also derived algebraically from Equation 1 for aromatic and anti-aromatic rings  
28 in the Supplementary Information. The wavelength of the lowest energy transition from the  
29  
30  
31  
32  
33  
34  
35  
36  
37  
38  
39  
40  
41  
42  
43  
44  
45  
46  
47  
48  
49  
50  
51  
52  
53  
54  
55  
56  
57  
58  
59  
60

HOMO-1 to the HOMO is then:

$$\lambda_N = hc/\Delta E = -hcN/4\pi\beta \quad (3)$$

showing that the transition wavelengths should shift linearly with  $N$ . The difference between the transition wavelengths for the  $N$  and  $N + 2$  rings is:

$$\Delta\lambda = -hc/2\pi\beta \quad (4)$$

Experimentally,  $\Delta\lambda$  is  $\approx 100$  nm, corresponding to  $\beta = -2$  eV.

For rings up to  $C_{28}^+$ , the crude Hückel model successfully predicts the observed linear trend for the origin wavelengths as a function of cluster size. However, the absorptions of the larger clusters,  $C_{30}^+$  to  $C_{36}^+$ , occur to longer wavelength than expected from the linear trend established for the smaller clusters ( $C_{14}^+$  to  $C_{28}^+$ ). For example, the  $C_{32}^+$ ,  $C_{34}^+$  and  $C_{36}^+$  bands lie 74, 154 and 92 nm to longer wavelength, respectively, compared to their expected positions based on the linear fit for the smaller clusters' wavelengths (see Figure 3). The origin of the departures from linearity is unclear, but may be associated with a progressive transition to polyynic structures with increasing cluster size.<sup>5,21,23,47</sup> Hot bands are another possible cause for shifting and broadening of the peaks with cluster size. As the rings become larger they should become increasingly floppy, so that even at cryogenic temperatures ( $T \approx 10$  K), low frequency ring deformation vibrational modes should be populated. Distortions from planar, circular structures may affect the electronic energies, such that the hot bands are displaced from the fundamental transitions. The lowest frequency ring deformation modes progressively diminish in frequency with increasing ring size so that hot bands should become more important for larger clusters. For example, DFT CAM-B3LYP-D3(BJ)/cc-pVDZ calculations predict that the four lowest frequency vibrational modes of  $C_{22}^+$  have frequencies of 6, 40, 52, and  $52 \text{ cm}^{-1}$ , whereas the four lowest frequency modes of  $C_{36}^+$  have frequencies of 5, 15, 20, and  $20 \text{ cm}^{-1}$ . Given that the QIT temperature is 10 K, one would

expect that only ring distortion vibrational modes with frequencies below  $\approx 20\text{ cm}^{-1}$  will be significantly populated (assuming a Boltzmann distribution). In principle, it should be possible in future experiments to explore the spectral consequences of exciting low frequency ring modes by recording electronic spectra of the clusters with the QIT held at different temperatures.

### Spectrum of $\text{C}_{14}^+$ - astrophysical implications and effect of tag atoms and molecules

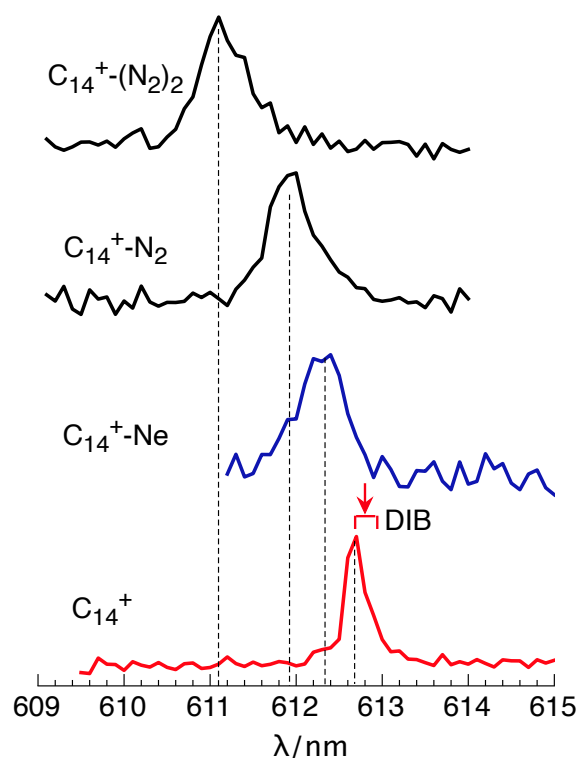


Figure 4: Electronic spectra of  $\text{C}_{14}^+$ ,  $\text{C}_{14}^+\text{-Ne}$ ,  $\text{C}_{14}^+\text{-N}_2$  and  $\text{C}_{14}^+\text{-(N}_2)_2$ . Spectra of  $\text{C}_{14}^+\text{-N}_2$ ,  $\text{C}_{14}^+\text{-(N}_2)_2$  and  $\text{C}_{14}^+\text{-Ne}$  were recorded by monitoring the photodepletion of the respective complex using 1-colour REPD. The spectrum of bare  $\text{C}_{14}^+$  was obtained by 2-colour REPD monitoring  $\text{C}_{11}^+$  photofragments. The wavelength and width for the weak 612.820 nm DIB reported in ref. 48 are indicated above the  $\text{C}_{14}^+$  plot.

The cyclo[ $n$ ]carbon cations are possible constituents of interstellar and circumstellar regions and may be detectable through their electronic transitions. Due to its relatively narrow



1  
2  
3 transitions the  $C_{14}^+$  ring is perhaps the best candidate for detection. As noted previously,<sup>24,25</sup>  
4 the relatively sharp  $C_{14}^+$  absorption lies close to a weak diffuse interstellar band (DIB) at  
5 612.820 nm with a width of 0.218 nm.<sup>48</sup> The current measurements confirm that the maxi-  
6 mum of the origin band for bare  $C_{14}^+$  is displaced by only 0.1 nm from the weak DIB (see  
7 Figure 4). The rotational temperature of the trapped  $C_{14}^+$  ions (10 K) is likely lower than for  
8 molecules in the interstellar medium (50–80 K), so that comparisons between astronomical  
9 and laboratory data requires spectra of bare  $C_{14}^+$  clusters for elevated ion trap temperatures  
10 to track the evolution of the band maximum and band contour with temperature.<sup>25</sup> If  $C_{14}^+$   
11 is indeed a DIB carrier, weaker peaks lying to shorter wavelengths at 604.2 nm ( $\approx \times 0.5$  the  
12 intensity of the 612.7 nm band) and at 602.9 nm ( $\approx \times 0.2$  the intensity of the 612.7 nm band),  
13 should also correspond to weak DIBs. Currently there are no appropriate matches for these  
14 peaks in published spectra of HD183143 or HD204827,<sup>48,49</sup> although the signal-to-noise ratio  
15 of astronomical spectra in the appropriate wavelength range may need to be improved for  
16 their detection.  
17  
18  
19  
20  
21  
22  
23  
24  
25  
26  
27  
28  
29  
30

31 Previous spectra of the cyclo[ $n$ ]carbon cations were recorded by forming and photodissoci-  
32 ating weakly-bound complexes of the target cyclo[ $n$ ]carbon cation tagged with He atoms<sup>25</sup> or  
33  $N_2$  molecules.<sup>24</sup> The band displacements caused by the tag atoms and molecules are clearly  
34 apparent in the spectra for  $C_{14}^+$ ,  $C_{14}^+-Ne$ ,  $C_{14}^+-N_2$  and  $C_{14}^+-(N_2)_2$  shown in Figure 4.  
35 The band maximum for the bare  $C_{14}^+$  ring lies at  $612.7 \pm 0.1$  nm, close to the wavelength  
36 (612.6 nm) deduced by Campbell *et al.* from  $C_{14}^+-He$  and  $C_{14}^+-He_2$  spectra, assuming that  
37 the spectral shifts caused by the first and second He atoms are additive.<sup>25</sup> Addition of He  
38 or Ne atoms shifts the  $C_{14}^+$  origin transition to higher energy by  $\approx 8$  and  $\approx 11$   $cm^{-1}$ , respec-  
39 tively. The shifts caused by  $N_2$  molecules are larger ( $+21$   $cm^{-1}/N_2$  molecule) and additive,  
40 consistent with structures in which the first two  $N_2$  molecules occupy equivalent sites above  
41 and below the  $C_{14}^+$  ring.<sup>24</sup> The conclusion is that spectral shifts caused by He, Ne and  $N_2$   
42 tags are relatively small, but are significant when transition wavelengths are to be compared  
43 with astronomical data.  
44  
45  
46  
47  
48  
49  
50  
51  
52  
53  
54  
55  
56  
57  
58  
59  
60

## Photodestruction of colossal carbon rings

We turn now to consider the photodestruction of cyclo[ $n$ ]carbon radical cations. From previous investigations, it is known that charged fullerene carbon clusters decompose mainly through loss of  $C_2$  molecules,<sup>29</sup> whereas smaller clusters with  $n \leq 20$  tend to lose  $C_3$  or  $C_5$  molecules.<sup>27,28,30,31</sup> In the intermediate size range  $20 \leq n \leq 40$  the photofragment distributions have been found to be sensitive to ion source conditions and laser power, suggesting that the cluster population contained different isomers, each with distinct absorption cross section and photodissociation behaviour.<sup>29</sup> Here we focus on even carbon rings ( $C_{14}^+$  to  $C_{36}^+$ ), and remove any structural ambiguity by selecting and probing only the ring isomer for each cluster size. Isomer selection is particularly important for the larger clusters. For example, for  $C_{30}^+$  the ring and bi-ring isomers have relative populations of 1:1, while for  $C_{36}^+$  the ring, bi-ring and fullerene isomers have relative populations of 1:3:3. We attempted to control the energy delivered to the clusters by using a two-photon resonance-enhanced excitation scheme (Figure 5a), whereby a relatively low power pulse of visible/NIR light ( $\leq 1$  mJ/cm<sup>2</sup>/pulse) tuned to the origin transition of the ring under examination was followed 10 ns later by a pulse of 230 nm UV light ( $\leq 1$  mJ/cm<sup>2</sup>/pulse). Intensities of the two beams were adjusted to limit the photodissociated fraction to  $\leq 10\%$  to reduce the effects of consecutive photon absorption. Assuming the clusters absorb one visible/NIR photon and one 230 nm photon, the total energy delivered to the clusters is 6.1–7.4 eV (the lower limit corresponds to  $C_{36}^+$  and the upper limit to  $C_{14}^+$ ). This energy should suffice to break the clusters into two fragments, but be insufficient to cause sequential fragmentation.<sup>39</sup> Photofragmentation mass spectra obtained under these conditions are shown in Figure 5b. The smaller clusters, up to  $C_{22}^+$ , tend to lose either a  $C_3$  or  $C_5$  unit, as observed in previous studies.<sup>27,30,31</sup> Rings larger than  $C_{26}^+$  also lose  $C_3$  or  $C_5$  units, but additionally produce  $C_{14}^+$ ,  $C_{18}^+$ , and  $C_{22}^+$  photofragments. These preferred larger cluster fragments would, if they were cyclic, have aromatic stability. To help understand the photofragment distributions apparent in Figure 5b, we calculated relative energies for different photofragment combinations. These

1  
2  
3  
4 energies are plotted in Figure 5c where it can be seen that the lower energy fragmentation  
5 channels correspond to the preferred photofragments apparent in Figure 5b. On energetic  
6 grounds, rings in the  $C_{28}^+ - C_{36}^+$  size range can be expected to break up into two smaller  
7 rings, one neutral and one charged, consistent with the photofragment mass spectra shown  
8 in Figure 5b. Similar fragmentation patterns are found for cyclo[ $n$ ]carbon cations subjected  
9 to collisional activation.<sup>10,11,50</sup>

10  
11  
12  
13  
14  
15 To investigate whether the larger charged photofragments are indeed cyclo[ $n$ ]carbons, we  
16 irradiated selected  $C_{28}^+$  rings in the QIT with a pulse of 235 nm light early in the trapping  
17 cycle to form photofragments that were subsequently tagged with  $N_2$  molecules (the trap gas  
18 for these experiments was a 1%  $N_2/He$  mixture) and recorded their electronic spectra with  
19 1-colour REPD. As an example, REPD spectra of  $N_2$ -tagged  $C_{14}^+$  and  $C_{18}^+$  clusters formed  
20 by photodissociating  $C_{28}^+$  ions in the QIT, are shown in Figure 6(a). The  $C_{14}^+$  and  $C_{18}^+$   
21 photofragment spectra are identical to the spectra of  $C_{14}^+$  and  $C_{18}^+$  produced directly by  
22 the laser ablation ion source,<sup>24</sup> proving that large  $C_{2n}^+$  rings predominately photodissociate  
23 to give smaller rings. Although, we have no information on the neutral co-fragments, they  
24 are almost certainly rings as the linear isomers lie much higher in energy.

25  
26  
27  
28  
29  
30  
31  
32  
33  
34  
35 We hypothesise that rupture of a large ring to generate two smaller rings follows a process  
36 whereby electronic excitation is followed by internal conversion to give a vibrationally ener-  
37 gized cluster which distorts and twists to form a bicyclic cluster that subsequently breaks  
38 into two smaller rings. Key steps along this pathway, calculated at the DFT CAM-B3LYP-  
39 D3(BJ)/cc-pVDZ level, are shown in Figure 6 for  $C_{28}^+$  disintegrating to  $C_{14}^+ + C_{14}$  ring  
40 fragments. In this case, the  $C_{14}^+ + C_{14}$  and  $C_{18}^+ + C_{10}$  fragment channels have simi-  
41 lar energies, consistent with the observation of strong  $C_{14}^+$  and  $C_{18}^+$  signals in the  $C_{28}^+$   
42 photofragment mass spectrum (Figure 5b).

43  
44  
45  
46  
47  
48  
49  
50  
51  
52  
53  
54  
55  
56  
57  
58  
59  
60  
Equipped with the distinctive electronic spectra for  $C_{2n}^+$  rings, we are in a position to  
assess the structures of the carbon cluster photofragments from other molecular systems,  
including charged PAHs, which upon exposure to light in ion traps, undergo progressive

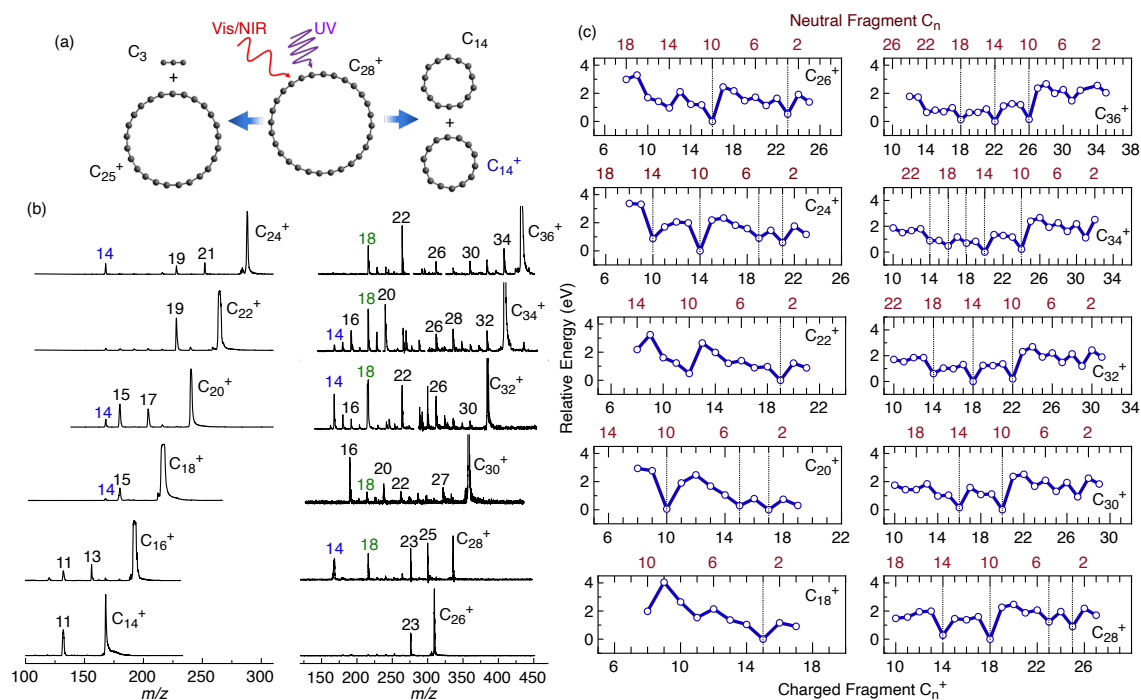


Figure 5: (a) Example of the two most significant photodissociation pathways for carbon rings in the C<sub>14</sub><sup>+</sup> to C<sub>36</sub><sup>+</sup> range: loss of neutral C<sub>3</sub> or C<sub>5</sub> molecules, and fragmentation to two rings, one neutral and one charged. (b) Photofragment mass spectra for isomer-selected C<sub>14</sub><sup>+</sup> to C<sub>36</sub><sup>+</sup> cyclo[n]carbons. The clusters were energized through resonance-enhanced two-photon excitation, with the first photon tuned to the cluster's main Vis/NIR transition ( $\leq 1$  mJ/cm<sup>2</sup>/pulse) and wavelength of the second photon fixed at 230 nm ( $\leq 1$  mJ/cm<sup>2</sup>/pulse). The numbers above the peaks indicate the number of carbon atoms in the photofragment cations. Loss of C<sub>3</sub> and C<sub>5</sub> neutrals for smaller clusters is augmented by loss of C<sub>10</sub>, C<sub>14</sub> and C<sub>18</sub> for larger clusters. Photofragment ToF mass spectra for the larger clusters were recorded in sections so that relative peak intensities are indicative rather than quantitative. (c) Relative energies for pairs of fragments from C<sub>2n</sub><sup>+</sup> (n=9–18) cyclic clusters calculated at the CAM-B3LYP-D3(BJ)/cc-pVDZ level. Fragments smaller than C<sub>10</sub><sup>+</sup> are linear, whereas larger fragments are cyclic. Energies for fragment pairs involving fullerenes, which may be important for C<sub>32</sub><sup>+</sup>, C<sub>34</sub><sup>+</sup> and C<sub>36</sub><sup>+</sup>, are not shown in the plot. The more stable product pairs are indicated by dotted vertical lines. Fragment energies are given in Table S1 in the SI.

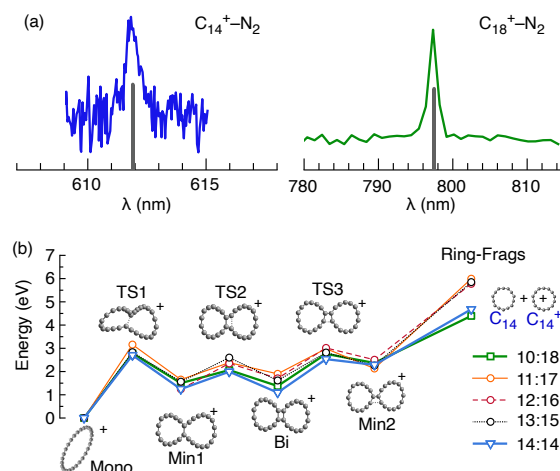


Figure 6: (a) Electronic spectra of  $C_{14}^+-N_2$  and  $C_{18}^+-N_2$  clusters that were generated by photodissociating  $C_{28}^+$  in the cryogenic ion trap to form  $C_{14}^+$  and  $C_{18}^+$  ions that were subsequently tagged with  $N_2$  molecules. The spectrum on the left was obtained by monitoring photodepletion of  $C_{14}^+-N_2$ , and the spectrum on the right by monitoring formation  $C_{18}^+$  from  $C_{18}^+-N_2$ . Vertical lines indicate transition wavelengths for  $C_{14}^+-N_2$  and  $C_{18}^+-N_2$  reported in ref. 24. (b) Structures on the path for dissociation of the  $C_{28}^+$  ring to give a pair of cyclic fragments. Structures and energies are calculated at the DFT CAM-B3LYP-D3(BJ)/cc-pVDZ level.

dehydrogenation to yield charged carbon clusters.<sup>15,16</sup> The chemical fate of PAHs subject to UV radiation is a crucial issue in regions of the interstellar medium.<sup>51</sup> The question is whether product carbon clusters, which include  $C_{14}^+$  and  $C_{18}^+$ , retain the structure of the PAH skeleton or whether they rearrange to become cyclo[ $n$ ]carbons, or perhaps some other low energy isomer.

Notably, the  $C_{34}^+$  and  $C_{36}^+$  rings also have a propensity for losing  $C_2$  units (see Figure 5), as does  $C_{32}^+$  to a lesser extent. The loss of  $C_2$  is a characteristic feature for the breakup of fullerenes induced by collisions or photon absorption,<sup>29,52–54</sup> but is less usual for  $C_n^+$  rings. Remembering that the photofragmentation mass spectra shown in Figure 5 were obtained for isomer-selected cyclo[ $n$ ]carbon cations, this raises the intriguing possibility that photoexcitation triggers a transformation of  $C_{34}^+$  and  $C_{36}^+$  rings to fullerenes with concomitant  $C_2$  loss(es) (and perhaps  $C_4$  and  $C_6$  losses). The process is akin to the transformation of planar rings to fullerenes that was deduced to occur when rings were subjected to energetic collisions

1  
2  
3 prior to analysis in an ion mobility spectrometer.<sup>52,53</sup> Exothermicities for conversion of rings  
4 to fullerenes + C<sub>2</sub> are predicted to be substantial. For example, using calculated energies  
5 given in Table S1 in the SI, the C<sub>36</sub><sup>+</sup>(ring)→C<sub>34</sub><sup>+</sup>(fullerene) + C<sub>2</sub> reaction is predicted to be  
6 exothermic by 6.3 eV. In contrast, the C<sub>36</sub><sup>+</sup>(ring)→C<sub>34</sub><sup>+</sup>(ring) + C<sub>2</sub> pathway is endothermic  
7 by 6.5 eV, and is probably less likely to occur.  
8  
9

10  
11 As a test, we also exposed isomer-selected C<sub>36</sub><sup>+</sup> fullerene clusters to pulses of 235 nm light  
12 and found that they strongly resisted photofragmentation compared to the ring isomers,  
13 consistent with the high C<sub>2</sub> binding energy (calculated to be 10.2 eV for the C<sub>36</sub><sup>+</sup> fullerene),  
14 and agreeing with previous observations that photodecomposition of fullerenes requires very  
15 high light intensities compared to other isomers.<sup>29</sup>  
16  
17  
18  
19  
20  
21  
22  
23  
24

## 25 Conclusions

26  
27 The current work demonstrates the power of gas-phase spectroscopy for elucidating the prop-  
28 erties of cyclo[*n*]carbon clusters. The outcomes of the work can be summarised as follows.  
29

30  
31 1. Electronic spectra of untagged, isomer-selected carbon cluster cations from C<sub>14</sub><sup>+</sup> to C<sub>36</sub><sup>+</sup>  
32 are obtained through two-colour action spectroscopy. Tag-free spectra of the carbon cluster  
33 cations are essential for comparisons with astronomical data and to judge the effects of at-  
34 tached tag atoms or molecules, which are not known *a priori*. The possibility of detecting  
35 C<sub>14</sub><sup>+</sup> in the interstellar medium is considered. The origin transition of bare C<sub>14</sub><sup>+</sup> at 612.7 nm  
36 lies 0.1 nm from a weak diffuse interstellar band at 612.82 nm. Further, spectroscopic studies  
37 are required to explore the effect of temperature on the band's position and shape. We  
38 present the first electronic spectra of C<sub>30</sub><sup>+</sup>, C<sub>32</sub><sup>+</sup>, C<sub>34</sub><sup>+</sup>, and C<sub>36</sub><sup>+</sup> cyclo[*n*]carbon cations.  
39 Despite C<sub>34</sub><sup>+</sup> and C<sub>36</sub><sup>+</sup> rings being far less stable than the fullerene isomers, by performing  
40 isomer-selective spectroscopy, we show that they survive at least ≈10<sup>6</sup> collisions with helium  
41 atoms at room temperature, and can be isolated and stored for relatively long periods of  
42 time (at least 1 s) in a cryogenic ion trap.  
43  
44  
45  
46  
47  
48  
49  
50  
51  
52  
53  
54  
55  
56  
57  
58  
59  
60

1  
2  
3  
4 2. We have developed a simple Hückel theory model to explain the linear shift of the wave-  
5 lengths for the  $C_{2n}^+$  absorption bands with cluster size. The model works well for clusters up  
6 to  $C_{28}^+$ , but begins to break down for larger clusters, perhaps due their increased floppiness,  
7 which may mean that they explore distorted geometries, even at cryogenic temperatures.  
8  
9

10  
11 3. Photofragmentation distributions are measured for isomer-selected carbon ring cations.  
12 Isomer selection is particularly important for clusters containing more than 20 carbon atoms,  
13 for which there are several isomers, each of which should have a characteristic photofrag-  
14 ment distribution. Smaller rings decompose by losing  $C_3$  and  $C_5$  molecules, while larger rings  
15 ( $C_{24}^+$  and larger), also break up into neutral and charged rings. The observed dissociation  
16 channels generally correspond to production of fragment pairs that are predicted through  
17 DFT calculations to lie lower in energy.  
18  
19

20  
21 4. To explore the photodecomposition of larger carbon rings, we trapped isomer-selected  
22  $C_{28}^+$  rings, exposed them to radiation, and then measured the electronic spectra of  $C_{14}^+$   
23 and  $C_{18}^+$  photofragments tagged with  $N_2$  molecules, confirming that these fragments are also  
24 rings. We proposed a mechanism for the fission of cyclic  $C_{28}^+$  based on DFT calculations,  
25 in which the penultimate fragmentation steps involve a bi-ring intermediate.  
26  
27

28  
29 5. Photoexcitation of  $C_{34}^+$  and  $C_{36}^+$  cyclo[ $n$ ]carbon isomers lead to loss of neutral  $C_2$  units,  
30 which may indicate that  $C_{34}^+$  and  $C_{36}^+$  cyclo[ $n$ ]carbons photoisomerise into fullerenes before  
31 dissociation. In principle, this transformation could be explored using a tandem ion mobil-  
32 ity mass spectrometer (IMS), with photo-excitation of selected rings following the first IMS  
33 stage and separation of photoproduct isomers in the second IMS stage, as described in ref.  
34  
35

36  
37 33. Photoconversion of carbon rings to fullerenes may be an important process in regions of  
38 the interstellar medium where stellar ultraviolet radiation is ubiquitous but where energetic  
39 collisions are infrequent due to low densities and temperatures.<sup>55</sup>  
40  
41

42  
43 There are several avenues for further work. Given that rings as large as  $C_{80}^+$  have been  
44 observed in ion mobility studies,<sup>13</sup> it would be interesting to continue spectroscopic studies to  
45 rings larger than  $C_{36}^+$ , following the trajectory of the band system further into the infrared  
46  
47  
48  
49  
50

1  
2  
3 where eventually it should have a similar energy to the ring's vibrational spacings. More  
4 structural information on the rings could also be derived from infrared spectra, particularly  
5 regarding the transition from cumulenic bonding in smaller cyclo[ $n$ ]carbons with equal C-C  
6 bond lengths to polyynic structures for larger clusters possessing alternating single and triple  
7 bonds.<sup>5,21,23,47</sup> Future spectroscopic studies will undoubtedly also target odd cyclo[ $n$ ]carbon  
8 cations ( $C_{2n+1}^+$ ).  
9  
10  
11  
12  
13  
14  
15  
16

## 17 Supporting Information Available

18  
19  
20 Supporting Information contains: (i) calculated ground state energies for cation and neutral  
21 carbon clusters, (ii) calculated dissociation energies of  $C_n^+$  clusters, (iii) calculated ionisation  
22 energies of  $C_n$  clusters, (iv) an analytical derivation of the Hückel theory model, and (v) *xyz*  
23 coordinates for calculated equilibrium geometries of  $C_n$  and  $C_n^+$  clusters.  
24  
25  
26  
27  
28  
29  
30

## 31 Acknowledgement

32  
33  
34 This research was supported under the Australian Research Council's Discovery Project  
35 funding scheme (Project Numbers DP150101427 and DP160100474). U. J. acknowledges  
36 support from the Swiss National Science Foundation (P2EZP2.178429). We thank Richard  
37 Mathys of the Science Faculty Workshop and Luke Weston for indispensable contributions  
38 to the design and construction of the apparatus. We thank Dr. Ewen Campbell for helpful  
39 discussions.  
40  
41  
42  
43  
44  
45  
46  
47

## 48 Conflict of Interest

49  
50  
51 The authors have no conflicts to disclose.  
52  
53  
54  
55  
56  
57  
58  
59  
60



## Data Availability Statement

The data that support the findings of this study are available from the corresponding author upon reasonable request.

## References

- (1) Kroto, H. W.; Heath, J. R.; O'Brien, S. C.; Curl, R. F.; Smalley, R. E. C<sub>60</sub>: Buckminsterfullerene. *Nature* **1985**, *318*, 162–163.
- (2) Weltner, W.; Van Zee, R. J. Carbon molecules, ions, and clusters. *Chem. Rev.* **1989**, *89*, 1713–1747.
- (3) Van Orden, A.; Saykally, R. J. Small carbon clusters: Spectroscopy, structure, and energetics. *Chem. Rev.* **1998**, *98*, 2313–2357.
- (4) Pitzer, K. S.; Clementi, E. Large molecules in carbon vapor. *J. Am. Chem. Soc.* **1959**, *81*, 4477–4485.
- (5) Anderson, H. L.; Patrick, C. W.; Scriven, L. M.; Woltering, S. L. A short history of cyclocarbons. *Bull. Chem. Soc. Jpn.* **2021**, *94*, 798–811.
- (6) Hahn, O.; Strassmann, F.; Mattauich, J.; Ewald, H. Hat in früheren Erdperioden ein radioaktives Cäsium existiert? Barium und Strontium aus Pollucit. *Naturwissenschaften* **1942**, *30*, 541–542.
- (7) McElvany, S. W.; Creasy, W. R.; O'Keefe, A. Ion–molecule reaction studies of mass selected carbon cluster ions formed by laser vaporization. *J. Chem. Phys.* **1986**, *85*, 632–633.
- (8) McElvany, S. W.; Dunlap, B. I.; O'Keefe, A. Ion molecule reactions of carbon cluster ions with D<sub>2</sub> and O<sub>2</sub>. *J. Chem. Phys.* **1987**, *86*, 715–725.

- 1  
2  
3  
4 (9) von Helden, G.; Hsu, M.; Kemper, P. R.; Bowers, M. T. Structures of carbon cluster  
5 ions from 3 to 60 atoms: Linears to rings to fullerenes. *J. Chem. Phys.* **1991**, *95*,  
6 3835–3837.  
7  
8  
9  
10 (10) von Helden, G.; Gotts, N. G.; Bowers, M. T. Annealing of carbon cluster cations: rings  
11 to rings and rings to fullerenes. *J. Am. Chem. Soc.* **1993**, *115*, 4363–4364.  
12  
13  
14 (11) Hunter, J. M.; Fye, J. L.; Jarrold, M. F. Annealing and dissociation of carbon rings. *J.*  
15 *Chem. Phys.* **1993**, *99*, 1785–1795.  
16  
17  
18 (12) von Helden, G.; Hsu, M. T.; Gotts, N.; Bowers, M. T. Carbon cluster cations with up  
19 to 84 atoms: Structures, formation mechanism, and reactivity. *J. Phys. Chem.* **1993**,  
20 *97*, 8182–8192.  
21  
22  
23  
24  
25 (13) Hunter, J. M.; Fye, J. L.; Roskamp, E. J.; Jarrold, M. F. Annealing carbon cluster ions:  
26 A mechanism for fullerene synthesis. *J. Phys. Chem.* **1994**, *98*, 1810–1818.  
27  
28  
29 (14) Lifshitz, C.; Peres, T.; Agranat, I. Properties of carbon cluster ions,  $C_n^+$ , formed by  
30 dissociative ionization. *Int. J. Mass. Spectrom. Ion Proc.* **1989**, *93*, 149–163.  
31  
32  
33  
34 (15) Ekern, S. P.; Marshall, A. G.; Szczepanski, J.; Vala, M. Photodissociation of gas-phase  
35 polycyclic aromatic hydrocarbon cations. *J. Phys. Chem. A* **1998**, *102*, 3498–3504.  
36  
37  
38  
39 (16) West, B.; Useli-Bacchitta, F.; Sabbah, H.; Blanchet, V.; Bodi, A.; Mayer, P. M.;  
40 Joblin, C. Photodissociation of pyrene cations: Structure and energetics from  $C_{16}H_{10}^+$   
41 to  $C_{14}^+$  and almost everything in between. *J. Phys. Chem. A* **2014**, *118*, 7824–7831.  
42  
43  
44  
45 (17) Hrodmarsson, H. R.; Bouwman, J.; Tielens, A. G. G. M.; Linnartz, H. Similarities  
46 and dissimilarities in the fragmentation of polycyclic aromatic hydrocarbon cations: A  
47 case study involving three dibenzopyrene isomers. *Int. J. Mass Spectrom.* **2022**, *476*,  
48 116834.  
49  
50  
51  
52  
53  
54  
55  
56  
57  
58  
59  
60

- 1  
2  
3  
4 (18) Diederich, F.; Rubin, Y.; Knobler, C. B.; Whetten, R. L.; Schriver, K. E.; Houk, K. N.;  
5 Li, Y. All-carbon molecules: Evidence for the generation of cyclo[18]carbon from a  
6 stable organic precursor. *Science* **1989**, *245*, 1088–1090.  
7  
8  
9  
10 (19) Kaiser, K.; Scriven, L.; Schulz, F.; Gawel, P.; Gross, L.; Anderson, H. An sp-hybridized  
11 molecular carbon allotrope, cyclo[18]carbon. *Science* **2019**, *365*, 1299–1301.  
12  
13  
14 (20) Xu, S.; Liu, F.; Xu, J.; Cui, Y.; Wang, C. Theoretical investigation on bond and  
15 spectrum of cyclo[18] carbon (C<sub>18</sub>) with sp-hybridized. *J. Mol. Model.* **2020**, *26*, 111.  
16  
17  
18 (21) Pereira, Z. S.; da Silva, E. Z. Spontaneous symmetry breaking in cyclo[18]carbon. *J.*  
19 *Phys. Chem. A* **2020**, *124*, 1152–1157.  
20  
21  
22  
23 (22) Hong, I.; Ahn, J.; Shin, H.; Bae, H.; Lee, H.; Benali, A.; Kwon, Y. Competition between  
24 Hückel's rule and Jahn-Teller distortion in small carbon rings: A quantum Monte Carlo  
25 study. *J. Phys. Chem. A* **2020**, *124*, 3636–3640.  
26  
27  
28  
29 (23) Baryshnikov, G. V.; Valiev, R. R.; Nasibullin, R. T.; Sundholm, D.; Kurten, T.;  
30 Ågren, H. Aromaticity of even-number cyclo[n]carbons ( $n=6-100$ ). *J. Phys. Chem.*  
31 *A* **2020**, *124*, 10849–10855.  
32  
33  
34 (24) Buntine, J. T.; Cotter, M. I.; Jacovella, U.; Liu, C.; Watkins, P.; Carrascosa, E.;  
35 Bull, J. N.; Weston, L.; Muller, G.; Scholz, M. S. et al. Electronic spectra of positively  
36 charged carbon clusters - C<sub>2n</sub><sup>+</sup> ( $n=6-14$ ). *J. Chem. Phys.* **2021**, *155*, 214302.  
37  
38  
39 (25) Rademacher, J.; Reedy, E. S.; Campbell, E. K. Electronic spectroscopy of monocyclic  
40 carbon ring cations for astrochemical consideration. *J. Phys. Chem. A* **2022**, *126*, 2127–  
41 2133.  
42  
43  
44 (26) Buntine, J. T.; Carrascosa, E.; Bull, J. N.; Jacovella, U.; Cotter, M. I.; Watkins, P.;  
45 Liu, C.; Scholz, M. S.; Adamson, B. D.; Marlton, S. J. P. et al. An ion mobility  
46  
47  
48  
49  
50  
51  
52  
53  
54  
55  
56  
57  
58  
59  
60

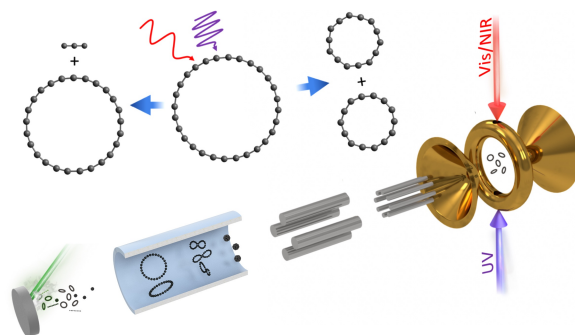
- 1  
2  
3 mass spectrometer coupled with a cryogenic ion trap for recording electronic spectra of  
4 charged, isomer-selected clusters. *Rev. Sci. Instr.* **2022**, *93*, 043201.  
5  
6  
7  
8 (27) Geusic, M. E.; McIlrath, T. J.; Jarrold, M. F.; Bloomfield, L. A.; Freeman, R. R.;  
9 Brown, W. L. Photofragmentation of mass-resolved carbon cluster ions: Observation  
10 of a “magic” neutral fragment. *J. Chem. Phys.* **1986**, *84*, 2421–2422.  
11  
12  
13 (28) Geusic, M. E.; Jarrold, M. F.; McIlrath, T. J.; Freeman, R. R.; Brown, W. L. Photodis-  
14 sociation of carbon cluster cations. *J. Chem. Phys.* **1987**, *86*, 3862–3869.  
15  
16  
17 (29) O’Brien, S. C.; Heath, J. R.; Curl, R. F.; Smalley, R. E. Photophysics of buckminster-  
18 fullerene and other carbon cluster ions. *J. Chem. Phys.* **1988**, *88*, 220–230.  
19  
20  
21 (30) Pozniak, B. P.; Dunbar, R. C. Photodissociation studies of  $C_n^+$  at 193 nm ( $n = 5-19$ ).  
22 *Int. J. Mass. Spectrom. Ion Proc.* **1997**, *165*, 299–313.  
23  
24  
25 (31) Dynak, N. J.; Rittgers, B. M.; Colley, J. E.; Kellar, D. J.; Duncan, M. A. Photofragment  
26 imaging of carbon cluster cations: Explosive ring rupture. *J. Phys. Chem. Lett.* **2022**,  
27 *13*, 4786–4793.  
28  
29  
30 (32) Moriyama, R.; Ohtaki, T.; Hosoya, J.; Koyasu, K.; Misaizu, F. Isomer-separated pho-  
31 todissociation of large sized silicon and carbon cluster ions: Drift tube experiment  
32 combined with a tandem reflectron mass spectrometer for  $Si_{24}^+$  -  $Si_{27}^+$  and  $C_{32}^+$ - $C_{38}^+$ . *Eur.*  
33 *Phys. J. D* **2013**, *67*, 1446–5.  
34  
35  
36 (33) Adamson, B. D.; Coughlan, N. J. A.; Markworth, P. B.; Continetti, R. E.; Bieske, E. J.  
37 An ion mobility mass spectrometer for investigating photoisomerization and photodis-  
38 sociation of molecular ions. *Rev. Sci. Instr.* **2014**, *85*, 123109.  
39  
40  
41 (34) Marlton, S. J. P.; Buntine, J. T.; Liu, C.; Watkins, P.; Jacovella, U.; Carrascosa, E.;  
42 Bull, J. N.; Bieske, E. J. Disentangling electronic spectra of linear and cyclic hydro-  
43  
44  
45  
46  
47  
48  
49  
50  
51  
52  
53  
54  
55  
56  
57  
58  
59  
60

- 1  
2  
3  
4 genated carbon cluster cations,  $C_{2n+1}H^+$  ( $n = 3-10$ ). *J. Phys. Chem. A* **2022**, *126*,  
5 6678–6685.  
6  
7
- 8 (35) Yanai, T.; Tew, D. P.; Handy, N. C. A new hybrid exchange–correlation functional  
9 using the Coulomb-attenuating method (CAM-B3LYP). *Chem. Phys. Lett.* **2004**, *393*,  
10 51–57.  
11  
12
- 13 (36) T. H. Dunning, Jr., Gaussian basis sets for use in correlated molecular calculations. I.  
14 The atoms boron through neon and hydrogen. *J. Chem. Phys.* **1989**, *90*, 1007.  
15  
16
- 17 (37) Grimme, S.; Ehrlich, S.; Goerigk, L. Effect of the damping function in dispersion cor-  
18 rected density functional theory. *J. Comput. Chem.* **2011**, *32*, 1456–1465.  
19  
20
- 21 (38) Frisch, M. J.; Trucks, G. W.; Schlegel, H. B.; Scuseria, G. E.; Robb, M. A.; Cheese-  
22 man, J. R.; Scalmani, G.; Barone, V.; Petersson, G. A.; Nakatsuji, H. et al. *Gaussian 16*,  
23 Revision C.01. Gaussian Inc.: Wallingford, CT, 2016.  
24  
25
- 26 (39) Sowa-Resat, M. B.; Hintz, P. A.; Anderson, S. L. Dissociation energies for small carbon  
27 cluster ions ( $C_{2-19}^+$ ) measured by collision-induced dissociation. *J. Phys. Chem.* **1995**,  
28 *99*, 10736–10741.  
29  
30
- 31 (40) Belau, L.; Wheeler, S. E.; Ticknor, B. W.; Ahmed, M.; Leone, S. R.; Allen, W. D.;  
32 Schaefer, H. F.; Duncan, M. A. Ionization thresholds of small carbon clusters: Tunable  
33 VUV experiments and theory. *J. Am. Chem. Soc.* **2007**, *129*, 10229–10243.  
34  
35
- 36 (41) Harper, O. J.; Boyé-Péronne, S.; Garcia, G. A.; Hrodmarsson, H. R.; Loison, J.-C.;  
37 Gans, B. To see  $C_2$ : Single-photon ionization of the dicarbon molecule. *J. Chem. Phys.*  
38 **2020**, *152*, 041105.  
39  
40
- 41 (42) Helden, G. v.; Hsu, M.; Gotts, N.; Kemper, P.; Bowers, M. Do small fullerenes exist  
42 only on the computer? Experimental results on  $C_{20}^{+/-}$  and  $C_{24}^{+/-}$ . *Chem. Phys. Lett.*  
43 **1993**, *204*, 15–22.  
44  
45  
46  
47  
48  
49  
50  
51  
52  
53  
54  
55  
56  
57  
58  
59  
60

- 1  
2  
3  
4 (43) Giuffreda, M. G.; Deleuze, M. S.; François, J. P. Structural, rotational, vibrational,  
5 and electronic properties of ionized carbon clusters  $C_n^+$  ( $n= 4-19$ ). *J. Phys. Chem. A*  
6 **1999**, *103*, 5137–5151.  
7  
8  
9  
10 (44) Fowler, P. W.; Mizoguchi, N.; Bean, D. E.; Havenith, R. W. A. Double aromaticity and  
11 ring currents in all-carbon rings. *Chem. Eur. J.* **2009**, *15*, 6964–6972.  
12  
13  
14 (45) Hückel, E. Quantentheoretische beiträge zum problem der aromatischen und  
15 ungesättigten verbindungen. III. *Z. Phys.* **1932**, *76*, 628–648.  
16  
17  
18  
19 (46) Frost, A. A.; Musulin, B. A mnemonic device for molecular orbital energies. *J. Chem.*  
20 *Phys.* **1953**, *21*, 572–573.  
21  
22  
23  
24 (47) Parasuk, V.; Almlöf, J.; Feyereisen, M. W. The [18] all-carbon molecule: cumulene or  
25 polyacetylene? *J. Am. Chem. Soc.* **1991**, *113*, 1049–1050.  
26  
27  
28  
29 (48) Hobbs, L. M.; York, D. G.; Thorburn, J. A.; Snow, T. P.; Bishof, M.; Friedman, S. D.;  
30 McCall, B. J.; Oka, T.; Rachford, B.; Sonnentrucker, P. et al. Studies of the diffuse  
31 interstellar bands. III. HD 183143. *Astrophys. J.* **2009**, *705*, 32.  
32  
33  
34  
35  
36 (49) Hobbs, L. M.; York, D. G.; Snow, T. P.; Oka, T.; Thorburn, J. A.; Bishof, M.; Fried-  
37 man, S. D.; McCall, B. J.; Rachford, B.; Sonnentrucker, P. A catalog of diffuse inter-  
38 stellar bands in the spectrum of HD 204827. *Astrophys. J.* **2008**, *680*, 1256.  
39  
40  
41  
42  
43 (50) Shelimov, K. B.; Hunter, J. M.; Jarrold, M. F. Small carbon rings: Dissociation, isomer-  
44 ization, and a simple model based on strain. *Int. J. Mass. Spectrom. Ion Proc.* **1994**,  
45 *138*, 17–31.  
46  
47  
48  
49  
50 (51) Tielens, A. G. G. M. Interstellar polycyclic aromatic hydrocarbon molecules. *Annu.*  
51 *Rev. Astron. Astrophys.* **2008**, *46*, 289–337.  
52  
53  
54  
55 (52) von Helden, G.; Gotts, N. G.; Bowers, M. T. Experimental evidence for the formation  
56  
57  
58  
59  
60

of fullerenes by collisional heating of carbon rings in the gas phase. *Nature* **1993**, *363*, 60–63.

- (53) von Helden, G.; Gotts, N. G.; Bowers, M. T. Annealing of carbon cluster cations: rings to rings and rings to fullerenes. *J. Am. Chem. Soc.* **1993**, *115*, 4363–4364.
- (54) Zhen, J.; Castellanos, P.; Paardekooper, D. M.; Linnartz, H.; Tielens, A. G. G. M. Laboratory formation of fullerenes from PAHS: Top-down interstellar chemistry. *Astrophys. J. Lett.* **2014**, *797*, L30.
- (55) Tielens, A. G. G. M. *The physics and chemistry of the interstellar medium*; Cambridge University Press: Cambridge, 2005.



TOC graphic